Liu *et al.*
Chinese Journal of Mechanical Engineering (2023) 36:114
https://doi.org/10.1186/s10033-023-00919-0

Chinese Journal of Mechanical Engineering

ORIGINAL ARTICLE

Open Access

Dynamic Recrystallization Behavior of Q370qE Bridge Steel

Caiyi Liu[1], Shicheng Liang[1], Yan Peng[1*], Jianliang Sun[1], Carlo Mapelli[2], Silvia Barella[2], Andrea Gruttadauria[2], Marco Belfi[2] and Ludovica Rovatti[2]

Abstract

Bridge steel has been widely used in recent years for its excellent performance. Understanding the high-temperature Dynamic Recrystallization (DRX) behavior of high-performance bridge steel plays an important role in guiding the thermomechanical processing process. In the present study, the hot deformation behavior of Q370qE bridge steel was investigated by hot compression tests conducted on a Gleeble 3800-GTC thermal-mechanical physical simulation system at temperatures ranging from 900 ℃ to 1100 ℃ and strain rates ranging from 0.01 s^{-1} to 10 s^{-1}. The obtained results were used to plot the true stress-strain and work-hardening rate curves of the experimental steel, with the latter curves used to determine the critical strains for the initiation of DRX. The Zener-Hollomon equation was subsequently applied to establish the correspondence between temperature and strain rate during the high-temperature plastic deformation of bridge steel. In terms of the DRX volume fraction solution, a new method for establishing DRX volume fraction was proposed based on two theoretical models. The good weathering and corrosion resistance of bridge steel lead to difficulties in microstructure etching. To solve this, the MTEX technology was used to further develop EBSD data to characterize the original microstructure of Q370qE bridge steel. This paper lays the theoretical foundation for studying the DRX behavior of Q370qE bridge steel.

Keywords Dynamic recrystallization, Materials characterization, Hot deformation, DRX volume fraction model

1 Introduction

High-performance bridge steel is widely used in cross-sea highways, high-speed railroads, and other projects due to its excellent properties, including high strength, high toughness, a low flexural strength ratio, easy welding, and corrosion resistance [1–3]. Bridge steel is mainly produced through a high-temperature rolling process. As the main softening mechanism in the process of the high-temperature plastic deformation of metal materials, dynamic recrystallization (DRX) is affected by the coupling interaction of temperature, strain rate, and strain. In turn, this coupling interaction determines the internal microstructure of the material, such as the grain size and morphology. DRX behavior significantly affects the mechanical properties of the product [4–6]. Therefore, the study of DRX behavior of the high-temperature plastic deformation of metallic materials plays an important role in revealing the mechanism of rolling microstructure evolution.

In recent years, the study of DRX behavior has received increasing attentions. Sellars et al. [7, 8] were the first to apply the Gleeble thermal-mechanical physical simulation machine to conduct a large number of experiments to establish a DRX model based on the Avrami function during the high-temperature rolling of metallic materials. Siciliano et al. [9] demonstrated the importance of the DRX of the high-temperature austenite phase in the hot rolling process for grain refinement. El-Shenawy et al. [10]

*Correspondence:
Yan Peng
pengyan@ysu.edu.cn
[1] National Engineering Research Center for Equipment and Technology of Cold Roll Strip Rolling, Yanshan University, Qinhuangdao 066004, China
[2] Department of Mechanical Engineering, Politecnico di Milano, 20156 Milan, Italy

verified the feasibility of the Gleeble-3500 physical simulation machine to simulate the microstructure transformation of materials during the rolling process. The researchers simulated the complex continuous rolling process via hot simulation experiments, showing that the physical simulation could effectively reduce the experiment and production costs. Fan et al. [11] studied the controlled rolling and cooling process of bridge steel. The results indicate that the microstructure is primarily composed of non-equiaxed ferrite grains with a martensite/austenite (M/A) constituent dispersed at the grain boundaries in specimens with heat-treatment on-line process temperature. The authors mainly focused on the phase transformation process during the rolling process of bridge steel and did not investigate the recrystallization behavior.

Duan et al. [12] investigated the DRX behavior of 34CrNiMo6 steel and developed a kinetic model for the DRX of the material based on the Avrami function. The researchers applied optical microscopy to characterize the microstructure evolution of the material during high-temperature deformation, and then predicted the DRX behavior of the material during high-temperature hot deformation using the deform finite element simulation. The results showed that the finite element simulation provides a theoretical guidance and process optimization for the metal material-forming process. Zhang et al. [13] studied the DRX behavior of magnesium-aluminum alloy during high-temperature plastic deformation, established a DRX volume fraction model based on traditional methods, and applied EBSD technology to analyze the microstructure transformation mechanism of DRX of magnesium-aluminum alloy. The researchers concluded that the type of DRX is related to the deformation temperature, and then applied Abaqus finite element simulation technology to simulate the grain size change law of magnesium-aluminum alloy during high-temperature plastic deformation. The results showed that the established model could better predict the microstructure change during material deformation. Wang et al. [14] studied the DRX behavior of 15V38 steel, determined the critical strain for DRX by analyzing the flow stress, and established the correspondence of DRX critical conditions using the Zener-Holloman equation. In addition, the researchers established the DRX volume fraction model and simulated the DRX volume fraction of the material by finite element simulation for the multi-pass rolling process. The results showed that the DRX volume fraction increased significantly with the increase of the deformation temperature. However, the researchers did not study the microstructure transformation mechanism under the high-temperature hot deformation of the material using the microstructure characterization technique.

Research on the recrystallization behavior of high-temperature plastic deformation of metallic materials has been mainly focused on the combination of kinetic modeling, microstructure characterization, and numerical simulation to study the DRX behavior of materials in high-temperature deformation process. Therefore, in this paper, the high-temperature flow behavior of bridge steel under different hot deformation parameters was obtained by hot compression experiments. Then, kinetic modeling was performed to predict the DRX volume fraction of bridge steel under different hot deformation parameters. The microstructure characterization of bridge steel was carried out using MTEX technology. This study provides a scientific basis for the design and optimization of the rolling process of bridge steel.

2 Experimental Materials and Methods

The material used in this experiment was commercial bridge steel Q370qE. The chemical composition and original microstructure of the experimental steel are shown in Table 1 and Figure 1, respectively. As shown in Figure 1, the original microstructure consisted of similarly sized grains. The average grain size was measured to be about 35 μm by using the intercept method. The Ac1 and Ac3 temperatures were determined from the dilatometric

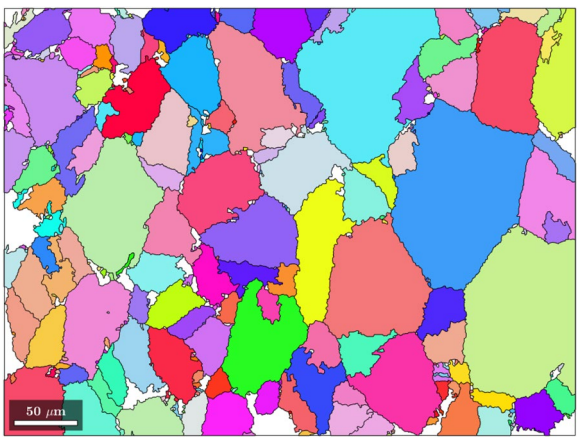

Figure 1 Reconstruction of the initial microstructure with MTEX technology

Table 1 Chemical composition of the steel (wt.%)

C	Mn	P	S	Si	Nb	Ti	Fe
0.16	1.5	0.01	0.003	0.2	0.04	0.015	Bal.

data obtained by the dilatometer DIL 402. As shown in Figure 2, Ac1 and Ac3 of the strip were determined to be 706 ℃ and 837 ℃, respectively. The experimental temperature was determined based on the obtained critical transition temperature. The equivalent substitution method was used to physically simulate the flexible rolling process with different rolling reductions. To study the material flow behavior during the high-temperature plastic deformation of the experimental steel, cylindrical specimens of 12 mm height and 8 mm diameter were cut from the strip. The flow behavior was measured in uniaxial compression using the Gleeble 3800-GTC thermal-mechanical physical simulation system. Prior to the experiment, the molybdenum disulfide lubricant was applied to both sides of the cylindrical sample. Tantalum foil with a thickness of 0.1 mm was placed between the anvil and specimen to reduce friction, avoid adhesion, and improve the stability and uniformity during deformation. The graphite was cut to a disc with a diameter 2 mm larger than the initial diameter of the specimen. Then, the disc was inserted between the anvil and the specimen to increase the electric resistance at the interface to achieve temperature uniformity over the specimen axis. A K type thermocouple was placed in the longitudinal center of the specimen to measure the temperature. The thermal simulation experimental procedure is shown in Figure 3a. The specimens were heated to 1150 ℃ at a heating rate of 10 ℃/s and held for 240 s to ensure the microstructure was uniformly austenitized. Then, the specimens were cooled to the deformation temperature at a cooling rate of 5 ℃/s and held for 60 s to eliminate the temperature gradient. Subsequently, the specimens were subjected to unidirectional hot compression experiments in an argon atmosphere with a reduction of 53%. Five temperatures (900 ℃, 950 ℃, 1000 ℃, 1050 ℃, and 1100 ℃) and four strain rates (0.01 s^{-1}, 0.1 s^{-1}, 1 s^{-1}, and 10 s^{-1}) were selected in the hot compression test to simulate the flexible rolling process, as shown in Figure 3b. To reserve the high-temperature initial austenite microstructure, the specimens were quenched immediately to room temperature after holding. The samples were cut along the axial direction. After mounting and polishing, the samples were vibrationally polished in the silica suspension solution for 2 h. The processed samples were analyzed using a Zeiss Sigma 500 scanning electron microscope (SEM) equipped with a HKL Channel 5 EBSD system to determine the morphologies and distributions of the grain boundaries. Due to the low carbon and phosphorus content of the specimen, it was difficult to etch the austenite

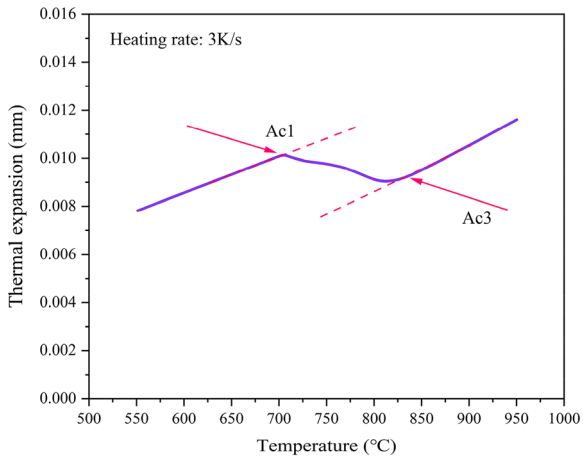

Figure 2 Variation in thermal expansion with temperature during the heating process of the experimental steel

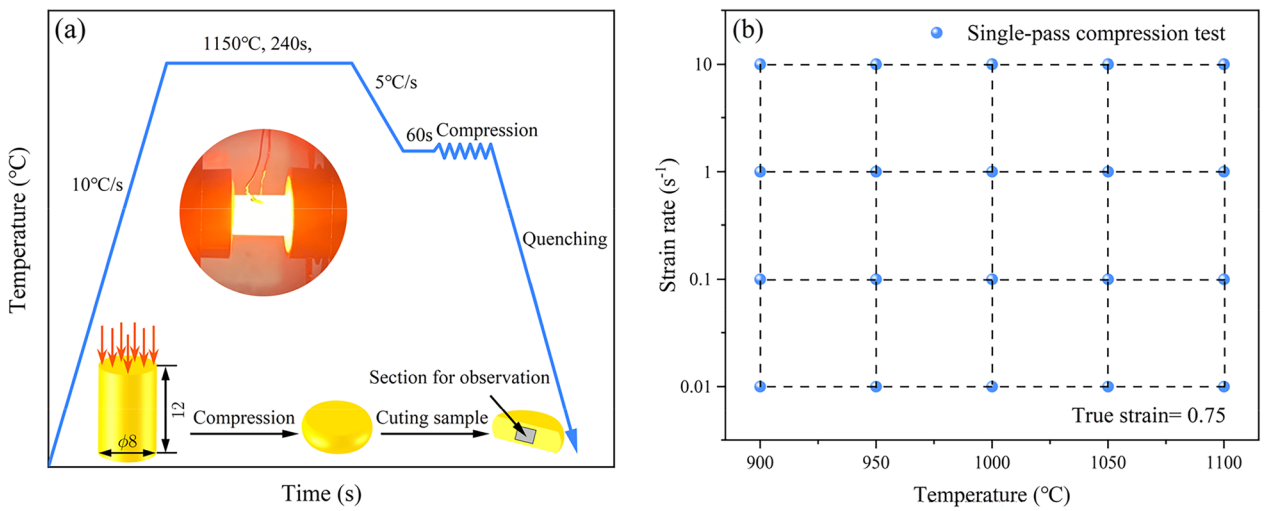

Figure 3 Experimental design: (**a**) Experimental procedure, (**b**) Deformation parameters

grain boundaries using Bechet-Beaujard method. In this paper, the MTEX methodology was used to further analyze the EBSD data to characterize the initial austenite microstructure.

3 Results and Discussion

3.1 Flow Stress Behavior

Figure 4 shows the flow stress curves of the experimental steel with different deformation conditions. From the figure, the flow stress varies with the deformation temperature and the strain rate. Under some deformation conditions, the flow stress curve had a peak stress, i.e., as the strain increased, the flow stress curve did not continue to increase, but instead tended to decrease and then reach a steady state. These results are consistent with the conclusions obtained from recent studies [15]. From Figure 4, the flow stress gradually decreased with the increase of the deformation temperature at a certain strain rate, and increased with the increase of the strain rate at a certain deformation temperature. For example, the peak stress decreased from 114.6 MPa at 900 °C to 42.6 MPa at 1100 °C with a strain rate of 0.01 s^{-1}. The peak stress increased from 114.6 MPa at 0.01 s^{-1} to 195.2 MPa at 10 s^{-1} with a deformation temperature of 900 °C. Some studies have shown that the DRX behavior of the material can be seen in the flow stress curves [16, 17]. To better understand the DRX behavior of materials on the flow stress curve, the material's flow stress curves during hot processing are shown in Figure 5. The work-hardening (WH), dynamic recovery (DRV), and dynamic recrystallization (DRX) behavior of the material during thermomechanical processing can be observed in Figure 5. DRV and DRX are the dynamic softening process during a thermomechanical processing process. In the early stages of deformation, due to the work-hardening effect, the stress increases rapidly with the increase of the

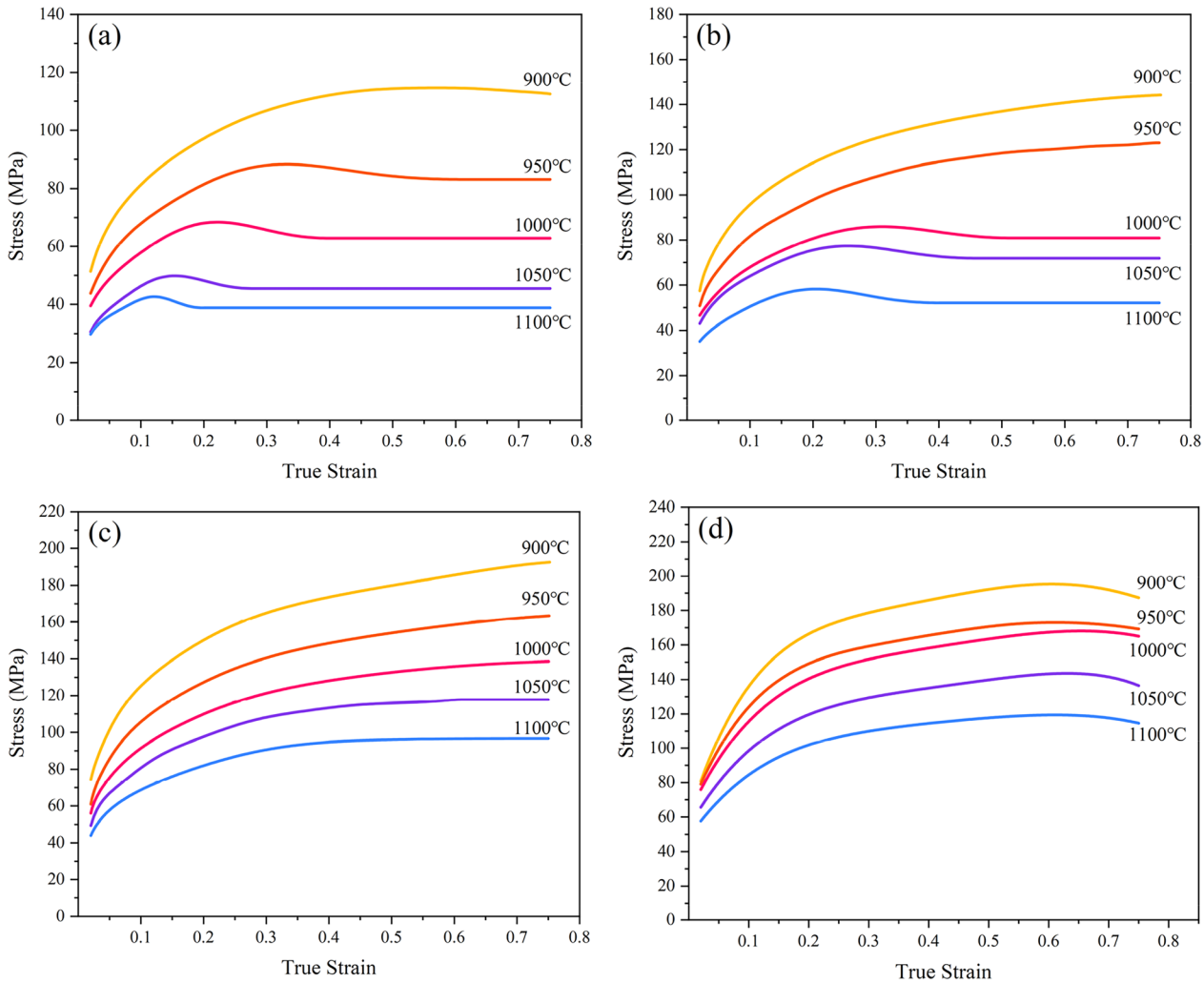

Figure 4 Flow stress curves under different deformation states: (**a**) 0.01 s^{-1}, (**b**) 0.1 s^{-1}, (**c**) 1 s^{-1}, (**d**) 10 s^{-1}

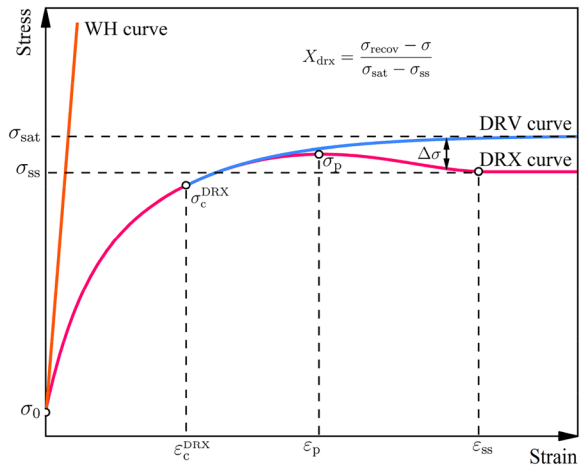

Figure 5 Schematic representations of the flow stress curves

strain. When the deformation reaches the critical state of dynamic recovery, dynamic recovery softening occurs, which is manifested as a slower rate of stress increase. When the deformation increases to the critical state of the DRX ε_c^{DRX}, the DRX softening occurs. After the flow stress reaches the peak stress σ_p, the flow stress decreases with an increase of strain. Finally, the flow stress reaches a stable state σ_{ss}, which indicates that the work hardening and dynamic softening have reached the dynamic equilibrium state. The DRX has the most significant softening effect on the material during hot processing. Therefore, understanding the DRX behavior of the material plays an important role in optimizing the rolling process and distributing the mill load.

From above analysis, the critical strain is a key parameter of the DRX. The critical strain mainly depends on the accumulated energy of the deformation process. In recent years, several methods have been proposed to identify the critical strain of the DRX [18–20]. Here, the mathematical modeling method was used to obtain the critical strain ε_c for the DRX. The procedure for deriving the critical strain involves drawing the work-hardening rate $\left|\mathrm{d}\sigma/\mathrm{d}\varepsilon\right|$ versus the σ curve. Then, the derivative of the work-hardening rate $\left|-\mathrm{d}\theta/\mathrm{d}\sigma\right|$ versus σ is calculated, and the minimum value is the inflection point of $\left|\mathrm{d}\sigma/\mathrm{d}\varepsilon\right| - \sigma$. Following this method, the critical strains of the DRX under different deformation conditions are shown in Figure 6. In the initial stage of the deformation, the material was mainly affected by the work-hardening rate and dynamic recovery, and the flow stress decreased slowly. This period represents the formation process of the subgrain microstructure [21]. When the strain reaches the DRX critical strain, the softening effect is greater, and the flow stress decreases rapidly. The DRX is the main softening mechanism of high-temperature plastic deformation, which results in a faster decrease in the flow stress until the work-hardening rate is zero, i.e., the peak stress σ_p is obtained. From Figure 6, the critical strain of the DRX decreased with the increase of the deformation temperature. When the critical strain is determined, the critical stress can be determined as well. From Figure 7, linear relationships between σ_p and σ_c, ε_p and ε_c can be observed at different deformation conditions.

During the high-temperature plastic deformation of materials, the hot deformation parameters (strain, stress, and strain rate) have an important influence on the DRX behavior [22–24]. The thermally activated storage energy during high-temperature plastic deformation is a key parameter to induce the DRX behavior of the material. Arrhenius-type models were used to illustrate the relationship between the thermally activated storage energy and the deformation behavior. The Zener-Hollomon (Z) parameter was designed to represent the coupling effect of the deformation temperature and the strain rate [25]:

$$Z = \dot{\varepsilon}\exp\left(\frac{Q}{RT}\right). \tag{1}$$

Sellars et al. [26, 27] proposed a hyperbolic sine function to indicate the relation among the thermodynamic parameters:

$$\begin{cases} A_1\sigma^{n_1}\exp\left(-\frac{Q}{RT}\right)(\alpha\sigma < 0.8, \text{low stress level}), \\ A_2\exp(\beta\sigma)\exp\left(-\frac{Q}{RT}\right)(\alpha\sigma > 1.2, \text{high stress level}), \\ A[\sinh(\alpha\sigma)]^n\exp\left(-\frac{Q}{RT}\right)(\text{all conditions}), \end{cases} \tag{2}$$

where A_1, A_2, A, n, n_1, and β are the materials constants; α is the stress multiplier, $\alpha \approx \beta/n_1$; Q is the activation energy for deformation (kJ/mol); $\dot{\varepsilon}$ is the strain rate (s^{-1}); T is the absolute temperature (K); R is the gas constant (8.314 J/mol); and σ is the flow stress (MPa). To facilitate the acquisition and calculation, the peak stress σ_p is generally used to represent σ. All the parameters in Eqs. (1)–(2) can be obtained using the natural algorithm method described in Refs. [25, 28, 29]. There are linear relationships between $\ln\dot{\varepsilon} - \ln\sigma_p$ and $\ln\dot{\varepsilon} - \sigma_p$, $\ln\left[\sinh\left(\alpha\sigma_p\right)\right] - 1/T$ and $\ln\dot{\varepsilon} - \ln\left[\sinh\left(\alpha\sigma_p\right)\right]$, as shown in Figure 8. The average slopes between $\ln\dot{\varepsilon}$ and $\ln\sigma_p$, $\ln\dot{\varepsilon}$ and σ_p were calculated: the material constant $n_1 = 7.998$, $\beta = 0.073\ \mathrm{MPa}^{-1}$. Then, α was obtained as 0.009. The activation energy Q for a constant strain rate can be expressed as:

$$Q = R\left|\frac{\partial\ln\dot{\varepsilon}}{\partial\ln[\sinh(\alpha\sigma)]}\right|_T\left\{\frac{\partial\ln\sinh(\alpha\sigma)}{\partial(1/T)}\right\}_{\dot{\varepsilon}}. \tag{3}$$

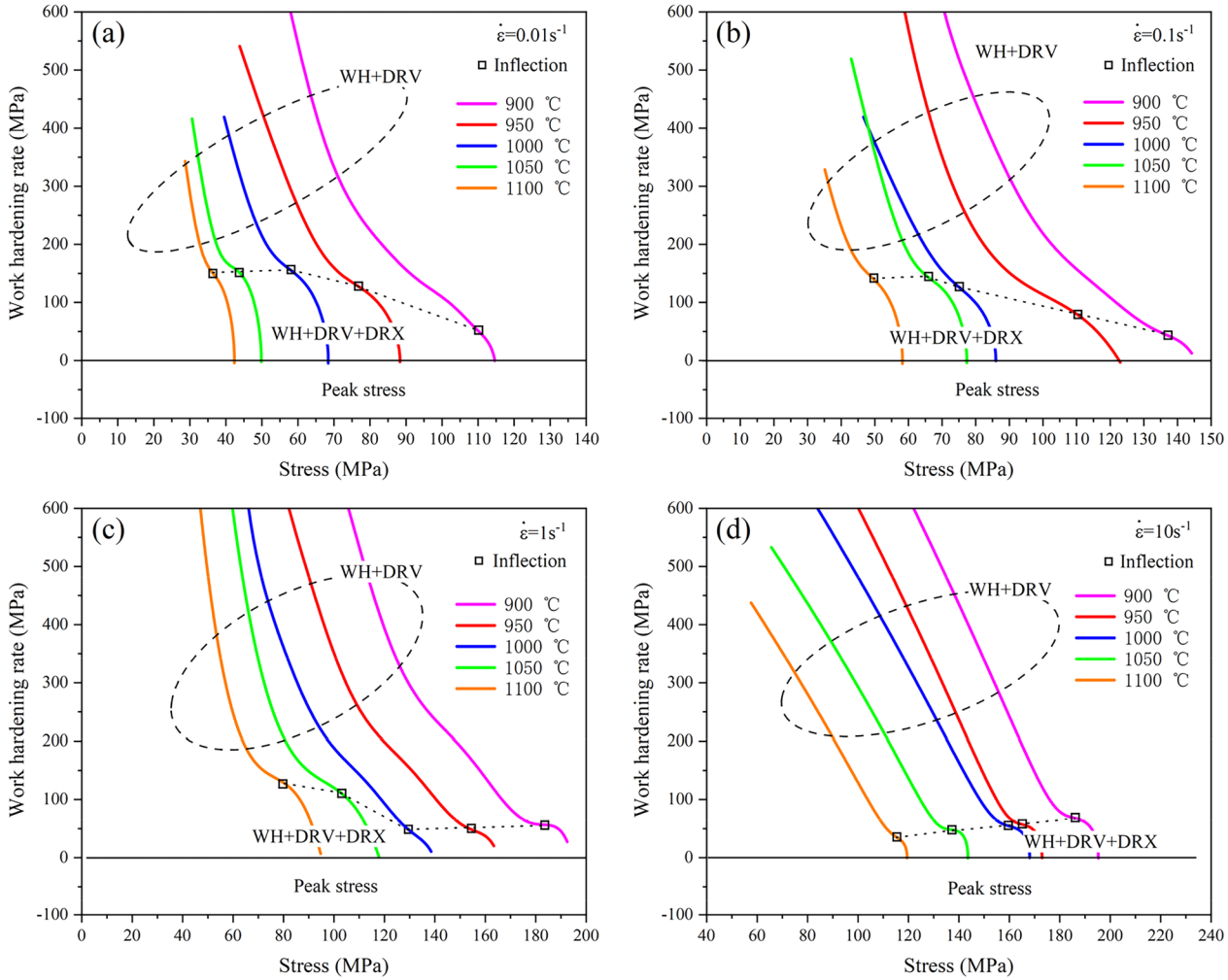

Figure 6 Work-hardening rate curves under different deformation states: (**a**) 0.01 s^{-1}, (**b**) 0.1 s^{-1}, (**c**) 1 s^{-1}, (**d**) 10 s^{-1}

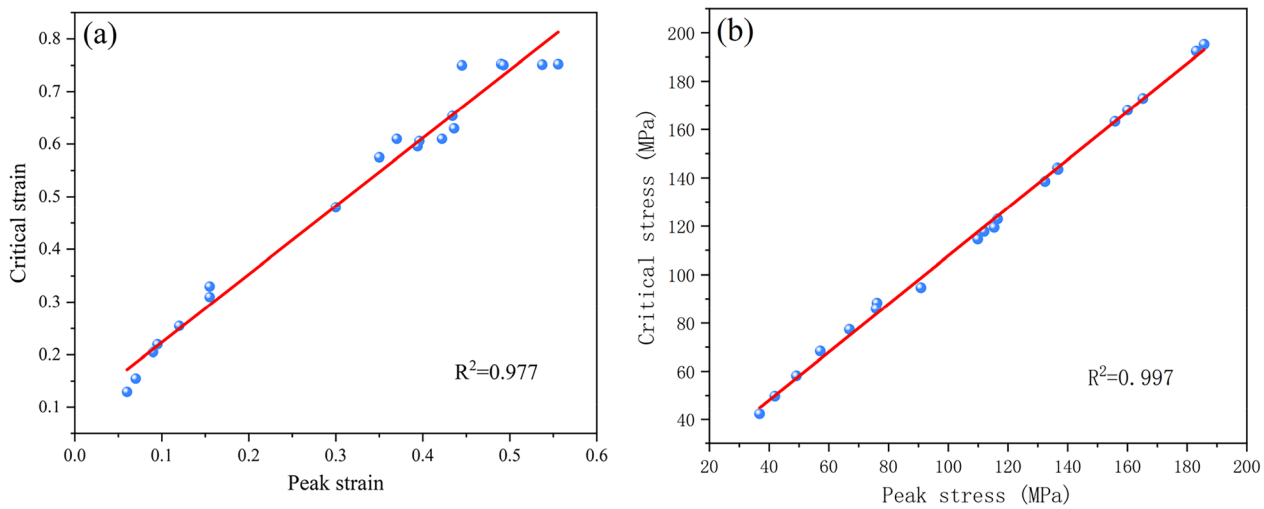

Figure 7 Relationship between peak state and critical state: (**a**) Peak strain versus critical strain, (**b**) Peak stress versus critical stress

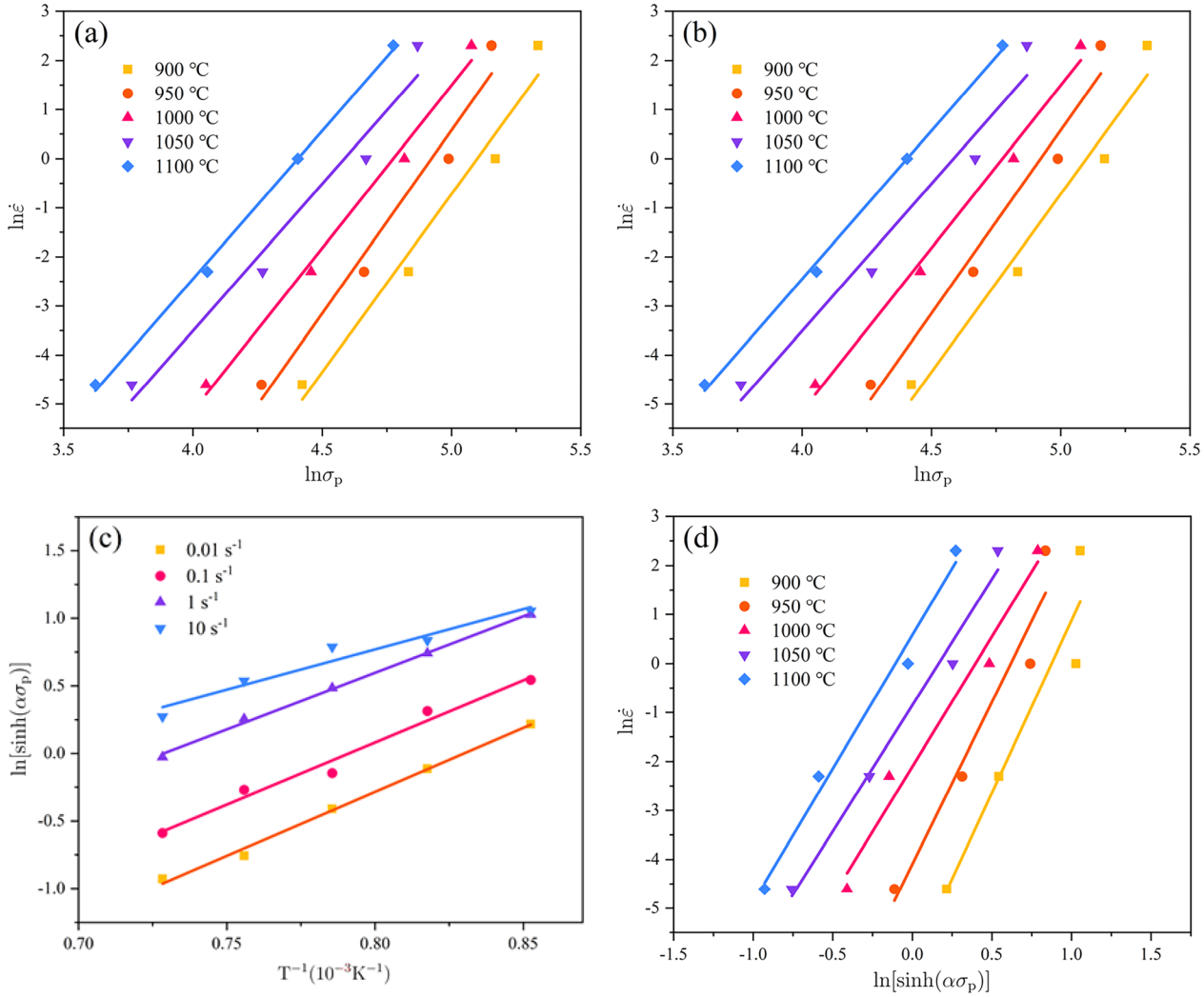

Figure 8 Linear regression fittings of (**a**) $\ln\dot{\varepsilon} - \ln\sigma_p$, (**b**) $\ln\dot{\varepsilon} - \sigma_p$, (**c**) $\ln\left[\sinh\left(\alpha\sigma_p\right)\right] - 1/T$, (**d**) $\ln\dot{\varepsilon} - \ln\left[\sinh\left(\alpha\sigma_p\right)\right]$

The average slopes between $\ln[\sinh(\alpha\sigma)]$ and $1/T$, and between $\ln\dot{\varepsilon}$ and $\ln[\sinh(\alpha\sigma)]$ were fitted out, as shown in Figure 8. The Q value was calculated to be 404.806 kJ/mol.

The natural logarithm function was used to calculate the last material constants A and n, which can be obtained based on the linear correlation between $\ln Z$ and $\ln\left[\sinh\left(\alpha\sigma_p\right)\right]$, as shown in Figure 9.

The values of A and n were found to be $A = 4.79 \times 10^{15}$ and $n = 5.789$, respectively. Eqs. (1) and (2) can be expressed as:

$$\dot{\varepsilon} = 4.79 \times 10^{15}[\sinh(0.009\sigma)]^{5.789}\exp\left(-\frac{404806}{RT}\right), \tag{4}$$

$$Z = \dot{\varepsilon}\exp\left(\frac{404806}{RT}\right) = 4.79 \times 10^{15}[\sinh(0.009\sigma)]^{5.789}. \tag{5}$$

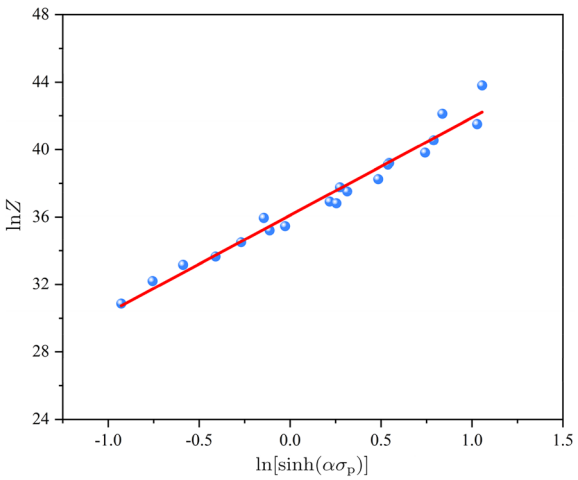

Figure 9 Linear regression fittings of $\ln Z$ and $\ln\left[\sinh\left(\alpha\sigma_p\right)\right]$

3.2 Establishment of the DRX Volume Fraction Model

DRX is a dynamic softening mechanism during the high-temperature plastic deformation of materials. There are many published studies on the calculation of DRX volume fraction [30–34]. Different physical parameters in DRX models represent different meanings, as explained in the above mentioned model calculation section, and it is noteworthy that some studies have used peak stress σ_p instead of saturation stress σ_{sat} [35, 36]. As discussed in the analysis in Section 3.1, the initiation point of the DRX is at the critical strain, and replacing the saturation stress σ_{sat} with the peak stress σ_p causes errors. In the model prediction analysis, the higher prediction DRX model depends on the internal softening mechanism of the DRX grains from the onset to the final evolution of the DRX. Therefore, it is appropriate to use the difference between the DRV saturation stress and steady stress as the DRX driving force. In this paper, a new DRX volume fraction model was proposed in combination with the methods proposed by Zahiri et al. [37] and Jonas et al. [38], as shown in Eq. (6):

$$X_{\mathrm{DRX}} = \frac{\sigma_{recov} - \sigma}{\sigma_{sat} - \sigma_{ss}}, \tag{6}$$

where X_{DRX} is the DRX experimental volume fraction, σ_{recov} is the DRV stress, σ is the flow stress, σ_{sat} is the saturation stress, and σ_{ss} is the steady state stress. σ and σ_{ss} can be determined from the flow stress curves. σ_{recov} can be calculated by the following equations:

$$\theta = \mathrm{d}\sigma/\mathrm{d}\varepsilon = s\sigma_{recov} + t, \tag{7}$$

$$s = -\theta_c(\sigma_{sat} - \sigma_c), \tag{8}$$

$$t = \theta_c\sigma_{sat}(\sigma_{sat} - \sigma_c), \tag{9}$$

where θ_c is the work-hardening rate corresponding to the critical stress. Then, σ_{recov} is estimated:

$$\sigma_{recov} = [(s\sigma_c + t)\exp(s\varepsilon - s\varepsilon_c) - t]/s. \tag{10}$$

The X_{DRX} can be calculated from the above equations to further develop the predicted DRX volume fraction. The following equation can be used to predict the DRX volume fraction under different deformation conditions [39]:

$$X_{\mathrm{DRX}} = 1 - \exp\left(-b\left(\frac{\varepsilon - \varepsilon_c}{\varepsilon_p}\right)^k\right), \tag{11}$$

where k and b are constants under different deformation conditions. Combining Eq. (11) with Eq. (6), the following equation can be obtained for the natural logarithms on both sides:

$$\ln[-\ln(1 - X_{\mathrm{DRX}})] = \ln b + k\ln\left(\frac{\varepsilon - \varepsilon_c}{\varepsilon_p}\right). \tag{12}$$

The above mathematical model allows to obtain the experimental and predicted DRX volume fraction under different deformation conditions. As shown in Figure 10, the predicted values were all highly consistent with the experimental value of the theoretical model. Figure 10, the DRX volume fraction was higher at lower strain rates. At a certain temperature, the DRX volume fraction gradually decreased with the increasing strain rate. The DRX volume fraction increased with the increasing temperature at a certain strain rate. At a lower strain rate and high temperature, the DRX volume fraction increased from 0 to 100%, indicating that a stable DRX process occurred. The increasing DRX volume fraction increasing rate underwent three stages: (1) The DRX volume fraction increased slowly with the increase of strain, (2) the DRX volume fraction rapidly increased, and (3) the DRX volume fraction increasing rate gradually decreased when the DRX volume fraction was close to 100%. For this kind of bridge steel, the deformed material acquires sufficient DRX behavior only at lower strain rates and higher temperatures. In this paper, the test steel exhibited significant DRX at the strain rate of 0.01 s^{-1}. Therefore, the average values of k and b were calculated from these deformation conditions [14]. The value of k was 2.2 and b was 1.6. Then, the predicted DRX model can be derived and expressed as:

$$X_{\mathrm{DRX}} = 1 - \exp\left(-1.6\left(\frac{\varepsilon - \varepsilon_c}{\varepsilon_p}\right)^{2.2}\right). \tag{13}$$

4 Conclusions

This paper investigated the Q370qE DRX behavior of bridge steel under different deformation conditions. The following conclusions were obtained:

(1) The flow stress curves of the experimental steel show that the DRX type curves were obtained at lower strain rates and higher temperatures. The peak stress of the flow stress curves varied with the hot deformation parameters.
(2) The critical strain ε_c and critical stress σ_c for DRX can be obtained from the work-hardening rate versus the stress curves during high-temperature plastic deformation. There are a linear relationships between the critical strain and peak strain, critical stress and peak stress.
(3) The average activation energy at the specified deformation conditions was 404.806 kJ/mol. The Zener-Hollomon equation was developed to describe the

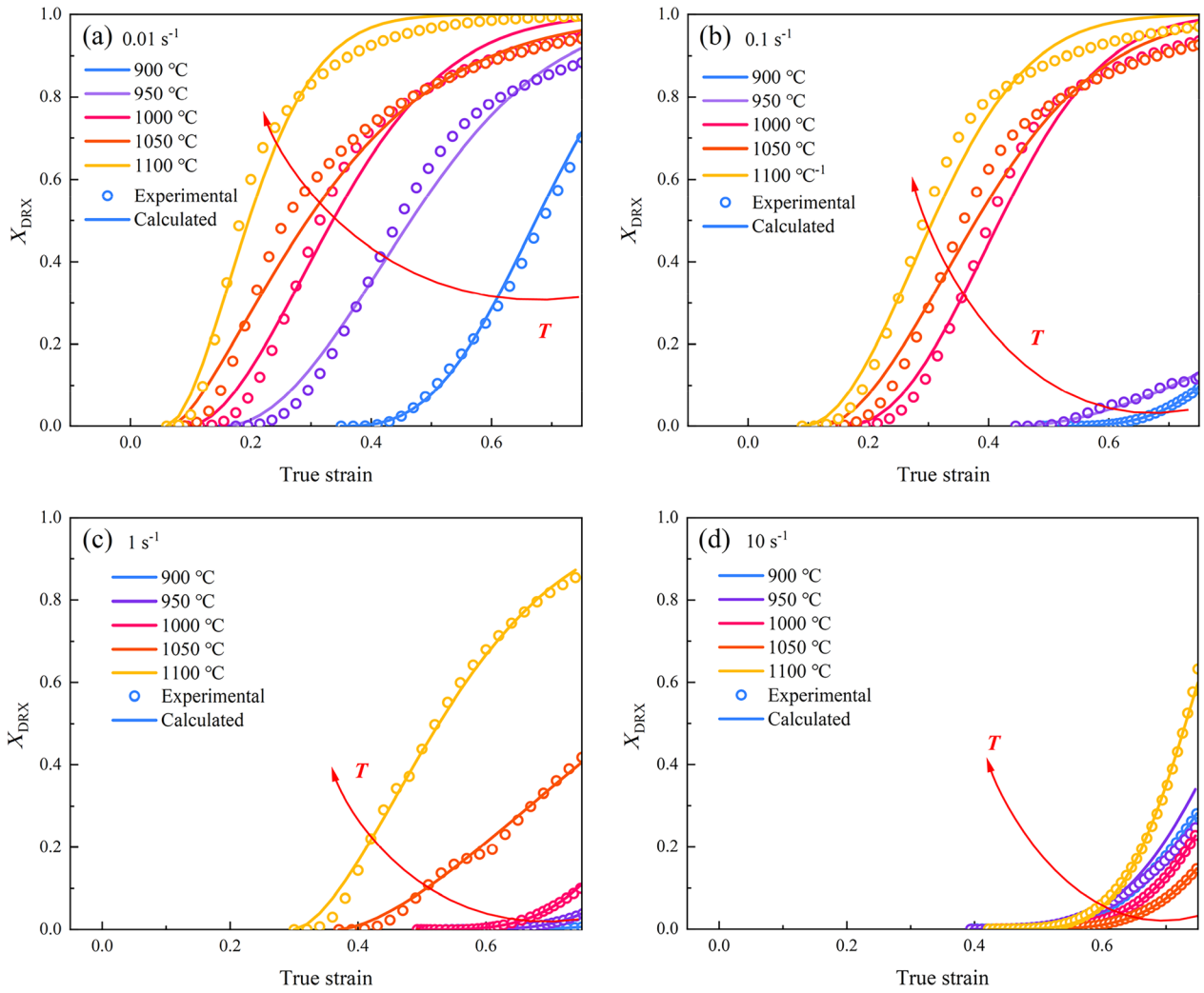

Figure 10 Comparison of the predicted and experimental X_{DRX} values

deformation behavior of the material with the coupling effect of the strain rate and temperature during high-temperature plastic deformation. $Z = \dot{\varepsilon}\exp\left(\frac{404806}{RT}\right) = 4.79 \times 10^{15}[\sinh(0.009\sigma)]^{5.789}$.

(4) A new predicted DRX model was proposed by combining the theoretical models. The experimental and predicted X_{DRX} values were compared. The new predicted DRX model has a formula of $X_{DRX} = 1 - \exp\left(-1.6\left(\frac{\varepsilon-\varepsilon_c}{\varepsilon_p}\right)^{2.2}\right)$, which in a good agreement with the experimental results.

Acknowledgements
Not applicable.

Authors' Contributions
CL was in charge of the whole trial and wrote the original manuscript. SL, AG, LR and MB assisted with sampling and laboratory analyses. YP and JS concepted the article and supported funding. CM and SB reviewed and edited original manuscript. All authors read and approved the final manuscript.

Authors' Information
Caiyi Liu, is an assistant professor at *School of Mechanical Engineering, Yanshan University, China*. His research interests include materials characterization and mechanical properties during flexible rolling process.
Shicheng Liang, is a master candidate at *School of Mechanical Engineering, Yanshan University, China*. His research interests include static recrystallization during flexible rolling process.
Yan Peng, is a professor at *School of Mechanical Engineering, Yanshan University, China*. His research interests include continuous strip rolling equipment-technology-product flexible adaptation and multi-objective synergistic control under instantaneous mutation.
Jianliang Sun, is a professor at *School of Mechanical Engineering, Yanshan University, China*. His research interests include intelligent monitoring and fault diagnosis of machinery and equipment.
Carlo Mapelli, is a professor at *Department of Mechanical Engineering, Politecnico di Milano, Italy*. His research interests include thermodynamics and kinetics of steel and metallurgical processes.
Silvia Barella, is an associate professor at *Department of Mechanical Engineering, Politecnico di Milano, Italy*. Her research interests include solidification

processes (casting and welding), hot and cold plastic deformation and the heat treatment of iron and aluminum based alloy.

Andrea Gruttadauria, is an associate professor at *Department of Mechanical Engineering, Politecnico di Milano, Italy*. His research interests include solidification processes of metal alloys (casting and welding of ferrous and nickel-based alloys), plastic deformation and thermal treatments of iron-based alloys, nickel and aluminum.

Marco Belfi, is a PhD candidate at *Department of Mechanical Engineering, Politecnico di Milano, Italy*. His research interests include heat treatment on the mechanical properties and microstructure of iron-based alloys, nickel and aluminum.

Ludovica Rovatti, is a senior technician at *Department of Mechanical Engineering, Politecnico di Milano, Italy*. Her research interests include etching technique for delineation of prior-austenite grain boundaries in carbon steels.

Funding

Supported by Regional Joint Funds of National Natural Science Foundation of China (Grant No. U20A20289), Hebei Provincial Innovative Research Groups Project of Natural Science Foundation of China (Grant No. E2021203011), General Program of National Natural Science Foundation of China (Grant Nos. 52075471, 52075473), Hebei Provincial Excellent Youth Science Foundation of China (Grant No. E2021203190), Hebei Provincial Innovative Capacity Cultivation Funding Project for Postgraduates of China (Grant No. CXZZSS2023040).

Declarations

Competing Interests

The authors declare no competing financial interests.

Received: 1 September 2021 Revised: 5 July 2023 Accepted: 21 July 2023
Published online: 11 October 2023

References

[1] B Qiang, X Liu, Y Liu, et al. Experimental study and parameter determination of cyclic constitutive model for bridge steels. *Journal of Constructional Steel Research*, 2021,183: 106738.

[2] X Han, D Y Yang, D M Frangopol. Optimum maintenance of deteriorated steel bridges using corrosion resistant steel based on system reliability and life-cycle cost. *Engineering Structures*, 2021, 243: 112633.

[3] X Liao, Y Wang, L Feng, et al. Investigation on fatigue crack resistance of Q370qE bridge steel at a low ambient temperature. *Construction and Building Materials*, 2020, 236: 117566.

[4] Y Wu, Z Liu, X Qin, et al. Effect of initial state on hot deformation and dynamic recrystallization of Ni-Fe based alloy GH984G for steam boiler applications. *Journal of Alloys and Compounds*, 2019, 795: 370-384.

[5] M Zhao, L Huang, C Li, et al. Evaluation of the deformation behaviors and hot workability of a high-strength low-alloy steel. *Materials Science and Engineering A*, 2021: 810.

[6] J Liu, X Wang, J Liu, et al. Hot deformation and dynamic recrystallization behavior of Cu-3Ti-3Ni-0.5Si alloy. *Journal of Alloys and Compounds*, 2019, 782: 224–234.

[7] C M Sellars, J A Whiteman. Recrystallization and grain growth in hot rolling. *Metal Science*, 1979, 13: 187-194.

[8] C M Sellars. Modelling microstructural development during hot rolling. *Materials Science and Technology*, 1990, 6(11): 1072-1081.

[9] F Siciliano, S F Rodrigues, Jr C Aranas, et al. The dynamic transformation of ferrite above AE3 and the consequences on hot rolling of steels. *Tecnologia em Metalurgia, Materiais e Mineração*, 2020, 17(2): 90-95.

[10] E H El-Shenawy. Physical simulation technology for thermo-mechanical processing of metallic alloys using Gleeble system. *Materials Today: Proceedings*, 2020, 28: 998-1004.

[11] L Fan, T Wang, Z Fu, et al. Effect of heat-treatment on-line process temperature on the microstructure and tensile properties of a low carbon Nb-microalloyed steel. *Materials Science and Engineering: A*, 2014, 607: 559-568.

[12] X W Duan, J J Liu, B Gong, et al. Experimental study and numerical simulation of dynamic recrystallization behavior of a high-strength steel. *Metals and Materials International*, 2021, 27(5): 1044-1059.

[13] C Zhang, C Wang, R Guo, et al. Investigation of dynamic recrystallization and modeling of microstructure evolution of an Al-Mg-Si aluminum alloy during high-temperature deformation. *Journal of Alloys and Compounds*, 2019, 773: 59-70.

[14] X Wang, K Chandrashekhara, S N Lekakh, et al. Modeling and simulation of dynamic recrystallization behavior in alloyed steel 15V38 during hot rolling. *Steel Research International*, 2019, 90(4): 1700565.

[15] R Zeng, L Huang, J Li, et al. Quantification of multiple softening processes occurring during multi-stage thermoforming of high-strength steel. *International Journal of Plasticity*, 2019, 120: 64-87.

[16] S Serajzadeh, A K Taheri. Prediction of flow stress at hot working condition. *Mechanics Research Communications*, 2003, 30(1): 87-93.

[17] R Yu, X Li, W Li, et al. Application of four different models for predicting the high-temperature flow behavior of TG6 titanium alloy. *Materials Today Communications*, 2021, 26: 102004.

[18] J Zou, J Chen, H Yan, et al. Effects of Sn addition on dynamic recrystallization of Mg-5Zn-1Mn alloy during high strain rate deformation. *Materials Science and Engineering A*, 2018, 735: 49-60.

[19] Y Han, S Yan, B Yin, et al. Effects of temperature and strain rate on the dynamic recrystallization of a medium-high-carbon high-silicon bainitic steel during hot deformation. *Vacuum*, 2018, 148: 78-87.

[20] P Zhang, C Yi, G Chen, et al. Constitutive model based on dynamic recrystallization behavior during thermal deformation of a nickel-based superalloy. *Metals*, 2016: 6(7).

[21] C Zhang, L Zhang, Q Xu, et al. The kinetics and cellular automaton modeling of dynamic recrystallization behavior of a medium carbon Cr-Ni-Mo alloyed steel in hot working process. *Materials Science and Engineering A*, 2016, 678: 33-43.

[22] Y Han, H Wu, W Zhang, et al. Constitutive equation and dynamic recrystallization behavior of as-cast 254SMO super-austenitic stainless steel. *Materials and Design*, 2015, 69: 230-240.

[23] X M Chen, Y C Lin, M S Chen, et al. Microstructural evolution of a nickel-based superalloy during hot deformation. *Materials and Design*, 2015, 77: 41-49.

[24] S Gu, L Zhang, C Zhang, et al. Modeling the effects of processing parameters on dynamic recrystallization behavior of deformed 38MnVS6 steel. *Journal of Materials Engineering and Performance*, 2015, 24(5): 1790-1798.

[25] Y Wang, J Wang, J Dong, et al. Hot deformation characteristics and hot working window of as-cast large-tonnage GH3535 superalloy ingot. *Journal of Materials Science and Technology*, 2018, 34(12): 2439-2446.

[26] C M Sellars. The kinetics of softening processes during hot working of austenite. *Czechoslovak Journal of Physics*, 1985, 35(3): 239-248.

[27] C M Sellars, W J McTegart. On the mechanism of hot deformation. *Acta Metallurgica*, 1966, 14(9): 1136-1138.

[28] X Zhang, L Huang, J Li, et al. Flow behaviors and constitutive model of 300M high strength steel at elevated temperature. *Journal of Central South University (Science and Technology)*, 2017, 48(6): 1439–1447.

[29] W Chuan, H Liang. Hot deformation and dynamic recrystallization of a near-beta titanium alloy in the β single phase region. *Vacuum*, 2018, 156: 384-401.

[30] C Li, Y Tan, F Zhao. Finite element simulation and process optimization of microstructure evolution in the formation of Inconel 718 alloy bolts. *Materials Research Express*, 2019, 6(2).

[31] L Lan, W Zhou, R D K Misra. Effect of hot deformation parameters on flow stress and microstructure in a low carbon microalloyed steel. *Materials Science and Engineering A,* 2019, 756: 18-26.

[32] H Vafaeenezhad, S H Seyedein, M R Aboutalebi, et al. An investigation of workability and flow instability of Sn-5Sb lead free solder alloy during hot deformation. *Materials Science and Engineering A*, 2018, 718: 87-95.

[33] N R Jaladurgam, A K Kanjarla. Hot deformation characteristics and microstructure evolution of Hastelloy C-276. *Materials Science and Engineering A*, 2018, 712: 240-254.

[34] A Hadadzadeh, F Mokdad, M A Wells, et al. Modeling dynamic recrystallization during hot deformation of a cast-homogenized Mg-Zn-Zr alloy. *Materials Science and Engineering A*, 2018, 720: 180-188.

[35] A I Fernández, P Uranga, B López, et al. Dynamic recrystallization behavior covering a wide austenite grain size range in Nb and Nb–Ti microalloyed steels. *Materials Science and Engineering: A*, 2003, 361(1): 367-376.
[36] M H Wang, Y F Li, W H Wang, et al. Chiba, quantitative analysis of work hardening and dynamic softening behavior of low carbon alloy steel based on the flow stress. *Materials and Design*, 2013, 45: 384-392.
[37] S H Zahiri, C H J Davies, P D Hodgson. A mechanical approach to quantify dynamic recrystallization in polycrystalline metals. *Scripta Materialia*, 2005, 52(4): 299-304.
[38] J J Jonas, X Quelennec, L Jiang, et al. The Avrami kinetics of dynamic recrystallization. *Acta materialia*, 2009, 57(9): 2748-2756.
[39] A Laasraoui, J Jonas. Recrystallization of austenite after deformation at high temperatures and strain rates—analysis and modeling. *Metallurgical Transactions A*, 1991, 22(1): 151-160.